Journal of Power Sources 229 (2013) 277–284

Contents lists available at SciVerse ScienceDirect

Journal of Power Sources

journal homepage: www.elsevier.com/locate/jpowsour

Highly active $Sm_{0.2}Ce_{0.8}O_{1.9}$ powders of very low apparent density derived from mixed cerium sources

Zhangbo Liu [a,b,1], Dong Ding [a,1], Mingfei Liu [a,1], Xiaxi Li [a], Wenping Sun [a,b], Changrong Xia [b], Meilin Liu [a,*]

[a] School of Materials Science and Engineering, Center for Innovative Fuel Cell and Battery Technologies, Georgia Institute of Technology, 771 Ferst Drive NW, Atlanta, GA 30332, United States

[b] CAS Key Laboratory of Materials for Energy Conversion, Department of Materials Science and Engineering, University of Science and Technology of China, Hefei, 230026 Anhui, China

HIGHLIGHTS

- Low apparent density SDC powders are derived from a GNP using mixed cerium precursors.
- High density and conductivity (~0.020 S cm^{-1} at 600 °C) SDC thin films are fabricated.
- Very high peak power density (0.725 W cm^{-2} at 600 °C) is demonstrated.

ARTICLE INFO

Article history:
Received 18 September 2012
Received in revised form
21 November 2012
Accepted 23 November 2012
Available online 30 November 2012

Keywords:
Ceria
Glycine–nitrate process
Electrolyte
Fuel cell
Solid oxide fuel cell

ABSTRACT

Low apparent density $Sm_{0.2}Ce_{0.8}O_{1.9}$ (SDC) powders of different morphology and microstructure are derived from a glycine–nitrate process using $Ce(NO_3)_3$ and $Ce(NH_4)_2(NO_3)_6$ as the cerium sources. When the molar ratio of the two cerium precursors is around 1:1, the derived SDC powders can be readily sintered to high density, exhibiting the highest conductivities (~0.084 and ~0.020 S cm^{-1} at 800 and 600 °C, respectively) with an activation energy of ~0.70 eV. When the molar ratio of $Ce(NO_3)_3$ to $Ce(NH_4)_2(NO_3)_6$ was adjusted to 3:1, the derived SDC powders have the lowest apparent density (36.0 ± 0.5 mg cm^{-3}), best suited for preparation of dense, thin-film SDC electrolyte membranes on porous anode substrates, a critical step toward low-cost fabrication of high-performance SOFCs.

1. Introduction

Solid oxide fuel cells (SOFCs) are regarded as one of the cleanest and most efficient devices for direct conversion to electricity of a wide variety of fuels, from hydrogen to hydrocarbons, coal gas, and bio-derived renewable fuels [1–7]. It is believed that broad application of SOFCs for power generation alone can significantly reduce pollutant emission and consumption of fossil fuels. Successful commercialization of SOFC technologies, however, has been constrained by many difficulties associated with the high operation temperatures (800–1000 °C). Thus, it is vital to lower the operation temperature of SOFCs to 700 °C or lower, so that much less expensive materials (e.g., low-cost steels) may be used as the interconnect and manifold components of SOFC systems with improved stability and reliability [1].

In recent years, considerable efforts have been devoted to the development of intermediate-temperature (IT) SOFCs based on thin-film electrolytes of doped ceria, which show much higher ionic conductivities than the state-of-the-art yttria-stabilized zirconia (YSZ) electrolytes at reduced temperatures [8,9]. For example, various complex vapor or solution deposition strategies have been studied for fabrication of thin-film SOFCs. While high quality thin electrolyte films have been produced, they are too expensive to be commercially viable. In contrast, a simple and elegant approach to fabrication of dense electrolyte films on porous anode substrates is a co-pressing and co-firing process, significantly reducing the fabrication cost [10,11]. However, the critical step of this process is the synthesis of electrolyte powders with extremely low apparent density, usually achieved via a glycine–nitrate process (GNP) [10–17].

* Corresponding author. Tel.: +1 404 894 6114; fax: +1 404 894 9140.
E-mail address: meilin.liu@mse.gatech.edu (M. Liu).
[1] These authors contribute equally to this work.

0378-7753/$ – see front matter © 2012 Elsevier B.V. All rights reserved.
http://dx.doi.org/10.1016/j.jpowsour.2012.11.082

GNP is a relatively inexpensive technique to synthesis fine and homogeneous powders, mainly based on the exothermicity of the reaction between glycine (the fuel) and nitrate (the oxidizer) [18]. In synthesis of doped ceria, $Ce(NO_3)_3$ is usually used as the cerium source while $Sm(NO_3)_3$ and $Gd(NO_3)_3$ are used as the doping precursor for $Sm_{0.2}Ce_{0.8}O_{1.9}$ (SDC) and $Gd_{0.1}Ce_{0.9}O_{1.95}$ (GDC), respectively [10,11]. Recently, the use of another precursor, $Ce(NH_4)_2(NO_3)_6$ ($Ce(IV)$), has attracted some attention for ceria synthesis [19–23], and different precursors may have significant impact on the properties of the resulting powders. For instance, Hwang et al. [20] used urea ($(NH_2)_2CO$) as the fuel and $Ce(NH_4)_2(NO_3)_6$ as both the source of cerium ion and the oxidizer to synthesize high-purity ceria powders via a dry combustion process. Yuan et al. showed that, through a hydrothermal route with the assistance of acetate, hydrophilic ceria nanocubes of 5 nm can be synthesized when $Ce(NH_4)_2(NO_3)_6$ was used as the precursor whereas those of 20 nm with $Ce(NO_3)_3$ [22]. To date, however, there is no comparative study concerning the effect of different ceria nitrate sources on powder properties, although other processing parameters (such as glycine/nitrate molar ratio and calcination temperature) have been extensively investigated as the main factors that affect the properties of ceria or doped-ceria powders synthesized by GNP [12,14,24,25].

In this paper, we report our findings on the effects of different cerium sources on the properties of SDC powders derived from GNP, focusing mainly on the apparent density and the specific morphology of powders as well as the ionic conductivity of sintered dense pellets and the performance of fabricated thin-film single cells. Mixed cerium nitrates with different mole ratio of $Ce(NO_3)_3$ to $Ce(NH_4)_2(NO_3)_6$ were studied as the starting materials to obtain SDC powders most suitable for IT-SOFC fabrication.

2. Experimental

2.1. Powder synthesis

Five kinds of $Sm_{0.2}Ce_{0.8}O_{1.9}$ (SDC) powders were derived from a GNP using $Sm(NO_3)_3\cdot 6H_2O$, $Ce(NO_3)_3\cdot 6H_2O$, and $Ce(NH_4)_2(NO_3)_6$ as precursors (all from Alfa Aesar). The details for each type of powder are presented in Table 1. In a typical synthesis experiment, stoichiometric amount of samarium ion and cerium ion containing nitrates were dissolved in distilled water to form a homogeneous solution, in which glycine (Alfa Aesar) was added as both the complexing agent and the fuel. To avoid possible impact of glycine/nitrate ratio, the glycine addition for each powder was fixed to the stoichiometric amount, which corresponds to the value when all glycine fuels are stoichiometrically oxidized by nitrates with only nitrogen, water, and carbon dioxide (CO_2) as gas products, which is widely reported to be the optimal value to produce high quality powders [12,14,25]. After stirring for half an hour to allow full complexation, the solution was then heated on a hotplate to ignite rapid self-sustaining combustion. The resulted ashes were subsequently calcined at 600 °C for 2 h to remove any carbon residues and to form crystalline SDC powders. For brevity, the five kinds of SDC powders are named as SDC-1, SDC-2, SDC-3, SDC-4, and SDC-5 thereafter, and the starting cerium sources as well as some properties of the powders are listed in Table 1.

2.2. Apparent density and conductivity measurement

The phase compositions of the powders were examined using X-ray diffraction analysis (XRD, X'Pert PRO Alpha-1, Cu Kα radiation), and the morphologies of the powders were characterized using a scanning electron microscope (SEM, LEO 1530). For SEM observation, powders were dispersed in ethanol and then drop-coated on an alumina substrate. The apparent density of the powders was estimated using an oscillating funnel method: (1) the powders were loaded into a funnel with a vibration device; (2) with a gentle vibration of the funnel, the powders began to free fall into a weighing bottle and filled it slowly in loose state; (3) the apparent density (ρ_a) can be calculated from the equation below:

$$\rho_a = m/V \quad (1)$$

where V is the volume of the container and m is the mass of the filling powders in the container.

To characterize the ionic conductivity, the as-prepared SDC powders were cold pressed under 250 MPa into cylindrical pellets (13 mm in diameter and ~1 mm in thickness) using a uniaxial die-press. These pellets were subsequently sintered at 1400 °C for 5 h with a heating rate of 3 °C min^{-1}. Then silver paste (Heraeus) was applied to both sides of the sintered pellets as electrodes for conductivity measurement. An EG&G PAR potentiostat (model 273A) coupled with a Solartron 1255 HF frequency response analyzer were used to measure the electrochemical impedance spectra (EIS) of the pellets in a frequency range from 100 kHz to 0.1 Hz with an *ac* amplitude of 10 mV. The measurement was conducted in the temperature range of 500–800 °C. The microstructures of the sintered pellets were characterized using a scanning electron microscope (SEM, LEO 1530) after grinding, polishing, and thermal etching (at 1000 °C for 2 h).

2.3. Single cell characterization

Bi-layer pellets consisting of porous NiO–SDC substrate and dense SDC electrolyte were fabricated using a co-pressing and co-sintering process [10,11]. NiO (prepared by GNP [26]) and SDC powders were mixed together to form the precursor of the anode substrate, in which starch (Sigma) was also added as pore former to increase the porosity. The mass ratio of NiO, SDC, and starch in the substrate was 65:35:15. The mixed powders were initially compacted at 50 MPa. Then a thin layer of SDC powders were uniformly distributed onto the pre-pressed substrate and uniaxially co-pressed to 250 MPa to form green bi-layer pellets, followed by

Table 1
Summary of starting cerium sources and some basic information of the SDC powders synthesized in this work.

Powder		SDC-1	SDC-2	SDC-3	SDC-4	SDC-5
Cerium sources	$Ce(NO_3)_3$	100 mol%	75 mol%	50 mol%	25 mol%	0 mol%
	$Ce(NH_4)_2(NO_3)_6$	0 mol%	25 mol%	50 mol%	75 mol%	100 mol%
Glycine/nitrate ratio		1.67	1.87	2.07	2.27	2.47
Apparent density (mg cm^{-3})		41.0 ± 0.5	36.0 ± 0.5	67.0 ± 0.5	107 ± 1	175 ± 1
Conductivity at 600 °C (S cm^{-1})		0.016	0.017	0.020	0.014	0.011
Activation energy at 500–800 °C (eV)		0.71	0.71	0.70	0.72	0.77
Fabricated cells		Cell-1	Cell-2	Cell-3	Cell-4	Cell-5

co-sintered at 1250 °C for 5 h to densify the electrolyte membrane. The sintered anode substrate thickness and diameter were 0.48 ± 0.01 mm and 11.0 ± 0.2 mm, respectively, while the thickness of the electrolyte membrane was about 22.5 ± 0.5 μm. Then, $Sm_{0.5}Sr_{0.5}CoO_3$ (SSC) (prepared by GNP [27]) and SDC powders with a mass ratio of SSC:SDC = 7:3 were mixed thoroughly with an organic binder (V-006, Heraeus) to form the cathode slurry, which was subsequently screen-printed onto the electrolyte surface of the sintered half cells, followed by firing at 950 °C for 2 h. The effective cathode area was 0.3 cm^2. For all the single cells, SDC powders contained in both electrodes were fixed to the most commonly used SDC-1, and the whole fabrication process was kept as consistent as possible so that identical electrode polarization resistance could be achieved.

Each single cell was sealed onto an alumina tube using ceramic adhesive (Aremco, Ceramabond 552). NiO paste (Heraeus) and silver paste (Heraeus) were employed as current collector on the anode and the cathode side, respectively, and Ag wire as the lead for both electrodes. Humidified (3% H_2O) hydrogen was fed to the anode at a flow rate of 30 mL min^{-1} as the fuel, while ambient air was used as the oxidant. In addition to measuring the current–voltage curve with an Arbin fuel cell testing system (MSTAT), the electrochemical impedance spectra were measured under open circuit conditions using an EG&G PAR potentiostat (model 273A) interface combined with a Solartron 1255 HF frequency response analyzer. The microstructures of the cells were examined using a scanning electron microscope (SEM, LEO 1530).

3. Results and discussions

3.1. Effect of glycine/nitrate ratio on powder synthesis

In the *glycine-nitrate process* (GNP), glycine is used as a complexing agent to prevent premature precipitation of metal ions and as the fuel for the subsequent combustion reaction. Accordingly, the glycine/nitrate ratio is critical to both the completion of the reaction between them and the properties of the resulting powders [28]. To examine the effects of different cerium sources, the glycine/nitrate ratio was kept at the most favorable stoichiometric one. However, this ratio varied slightly for powders derived from different combination of precursors, due to the difference in the valence state of cerium in different precursors. Assuming that the only products of the reactions are the desired SDC phase, nitrogen, water, and carbon dioxide (CO_2), and the oxidation of Ce(III) (from $Ce(NO_3)_3$) to form Ce(IV) was resulted from O_2 in air. Complete combustion reactions between nitrates and glycine for each type of SDC powder can be expressed as follows (together with the stoichiometric glycine/nitrate ratios):

SDC-1:

$$1/5Sm(NO_3)_3 + 4/5Ce(NO_3)_3 + 5/3NH_2 - CH_2 - COOH + 1/5O_2 \rightarrow SDC\text{-}1 + 7/3N_2 + 25/6H_2O + 10/3CO_2 \quad (2)$$
$$(\text{glycine/nitrate} = 5/3 \approx 1.67)$$

SDC-2:

$$1/5Sm(NO_3)_3 + 3/5Ce(NO_3)_3 + 1/5Ce(NH_4)_2(NO_3)_6 + 28/15NH_2 - CH_2 - COOH + 3/20O_2 \rightarrow SDC\text{-}2 + 44/15N_2 + 82/15H_2O + 56/15CO_2 \quad (\text{glycine/nitrate} = 28/15 \approx 1.87) \quad (3)$$

SDC-3:

$$1/5Sm(NO_3)_3 + 2/5Ce(NO_3)_3 + 2/5Ce(NH_4)_2(NO_3)_6 + 31/15NH_2 - CH_2 - COOH + 1/10O_2 \rightarrow SDC\text{-}3 + 53/15N_2 + 203/30H_2O + 62/15CO_2 \quad (\text{glycine/nitrate} = 31/15 \approx 2.07) \quad (4)$$

SDC-4:

$$1/5Sm(NO_3)_3 + 1/5Ce(NO_3)_3 + 3/5Ce(NH_4)_2(NO_3)_6 + 34/15NH_2 - CH_2 - COOH + 1/20O_2 \rightarrow SDC\text{-}4 + 62/15N_2 + 121/15H_2O + 68/15CO_2 \quad (\text{glycine/nitrate} = 34/15 \approx 2.27) \quad (5)$$

SDC-5:

$$1/5Sm(NO_3)_3 + 4/5Ce(NH_4)_2(NO_3)_6 + 37/15NH_2 - CH_2 - COOH \rightarrow SDC\text{-}5 + 71/15N_2 + 281/30H_2O + 74/15CO_2 \quad (\text{glycine/nitrate} = 28/15 \approx 2.47) \quad (6)$$

The actual glycine/nitrate ratio for each powder was kept at the stoichiometric ratio shown in the above Eqs. (2)–(6).

3.2. Properties of synthesized powders

After calcination at 600 °C for 2 h, all the SDC powders exhibit a single-phase fluorite structure, as shown in Fig. 1, confirming the feasibility of utilizing $Ce(NO_3)_3$ and/or $Ce(NH_4)_2(NO_3)_6$ as the precursors. The morphologies of the powders are shown in Fig. 2. Clearly, all powder samples consist of aggregates of small particles due to significant agglomeration (and some degree of sintering) of primary particles during combustion. When $Ce(NO_3)_3$ was used as the cerium source, the resulting aggregates (or foam powders) of SDC-1 appear highly porous with cage-like structure, similar to those synthesized by Xia and Liu [10]. In contrast, when $Ce(NH_4)_2(NO_3)_6$ was used as the cerium source, the obtained aggregates (or foam powders) of SDC-5 look much denser (see Fig. 2(e)) than SDC-1 due to even stronger agglomeration of primary particles. The use of mixed cerium sources resulted in different morphologies with varying degree of agglomeration, porosity, and pore size. In particular, when the molar ratio of $Ce(NH_4)_2(NO_3)_6$ to $Ce(NO_3)_3$ was 1:3, the cage-like structure was changed to an O-shape structure

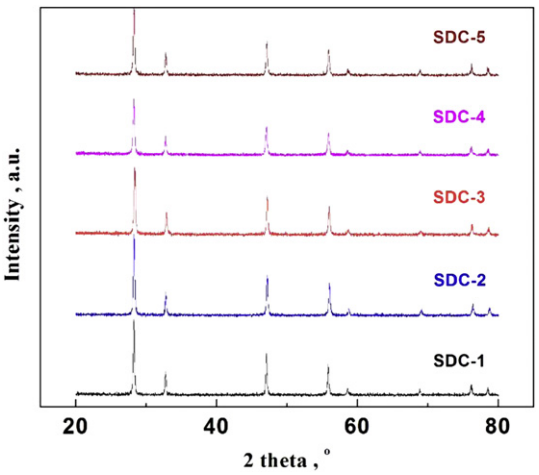

Fig. 1. XRD patterns of SDC powders derived from different cerium sources after calcination at 600 °C for 2 h.

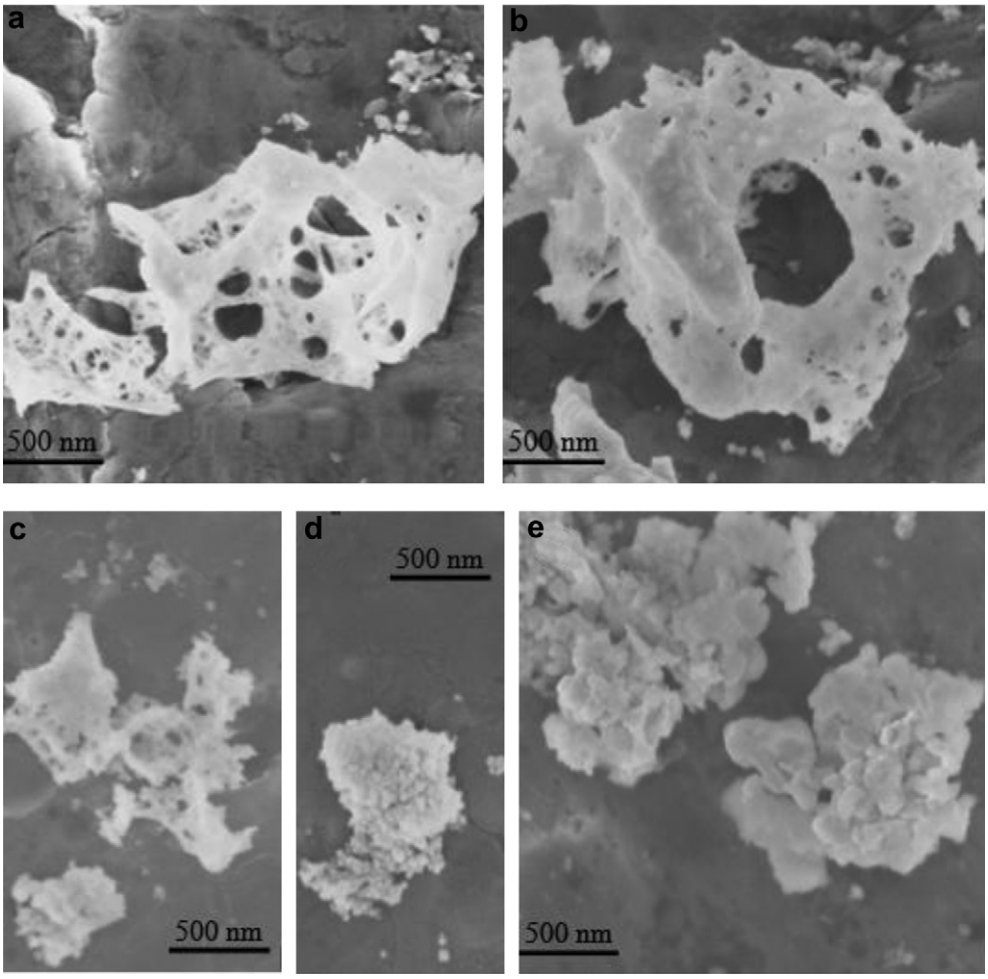

Fig. 2. SEM images of the synthesized SDC powders: (a) SDC-1, (b) SDC-2, (c) SDC-3, (d) SDC-4, and (e) SDC-5.

with a large pore at the center of each aggregate, in addition to lots of small pores. These morphological features of the resulting SDC powders are originated from the cerium precursors used in the GNP synthesis, which determine the properties of the powders (e.g., apparent density, specific surface area, and sintering behavior) and, thus, the properties of the electrolyte membranes.

Shown in Fig. 3(a) is a visual comparison in volume of the SDC powders (same weight, 1.00 g) when they were free fell into the weighing bottle using the oscillating funnel method. The apparent densities of the powders, calculated using Eq. (1) and shown in Fig. 3(b), increased with the content of $Ce(NH_4)_2(NO_3)_6$ used in the mixture (except SDC-2, which has the lowest value of 36.0 ± 0.5 mg cm^{-3}). This is consistent with the apparent densities of the aggregates shown in Fig. 2. Since the theoretical density of SDC is about 7.15 g cm^{-3}, the apparent densities of the powders synthesized in this study are all less than 2.45% of the theoretical value (SDC-5 has the highest apparent density of $\sim 175 \pm 1$ mg cm^{-3}). In particular, the apparent density of SDC-2 is only about 0.50% of the theoretical value, even lower than that reported by a previous study using a novel PVA assisted self-rising approach [29]. The low apparent density of SDC-2 is attributed to the unique O-shape porous morphology of the foam powder. There is no doubt that foam powders with lower apparent bulk density is more favorable for the fabrication of thin and dense electrolyte membrane on a porous anode substrate by a dry pressing process. With the SDC-2 powders, dense SDC electrolyte films as thin as $\sim$4.0 μm have been successfully fabricated on a NiO–SDC substrate using a co-pressing and co-sintering process, as shown in Fig. 3(c).

Further, high ionic conductivity is another important requirement of SDC powders for fabrication of low-temperature SOFC electrolyte membranes. Shown in Fig. 4 are the ionic conductivities of the SDC pellets fabricated from different powders (sintered at 1400 °C for 5 h), as determined from impedance spectra acquired at 500–800 °C. Clearly, the conductivities of the sample SDC-1 are higher than those of SDC-5, indicating that $Ce(NO_3)_3$ is superior to $Ce(NH_4)_2(NO_3)_6$ as a cerium source for synthesis of SDC powders using the GNP. Moreover, it is found that the use of a mixture of $Ce(NO_3)_3$ and $Ce(NH_4)_2(NO_3)_6$ as the cerium source led to significant increase in ionic conductivities because the conductivities of SDC-2 are higher than those of SDC-1 while SDC-4 shows higher conductivities than SDC-5 in the temperature range studied. In particular, SDC-3 showed the highest conductivities, reaching $\sim$0.084 and $\sim$0.020 S cm^{-1} at 800 and 600 °C, respectively.

The temperature dependence of electrical conductivities of each powders are shown in Fig. 4(c); the activation energies were calculated from the slops of the Arrhenius plots, ln (σT) versus 1000/T. It is also noted that the activation energies for ionic conduction are relatively low for all samples except SDC-5 ($\sim$0.77 eV). Electrolyte materials with lower activation energy have more potential to display high performance at reduced temperatures. Moreover, the activation energy appears to decrease

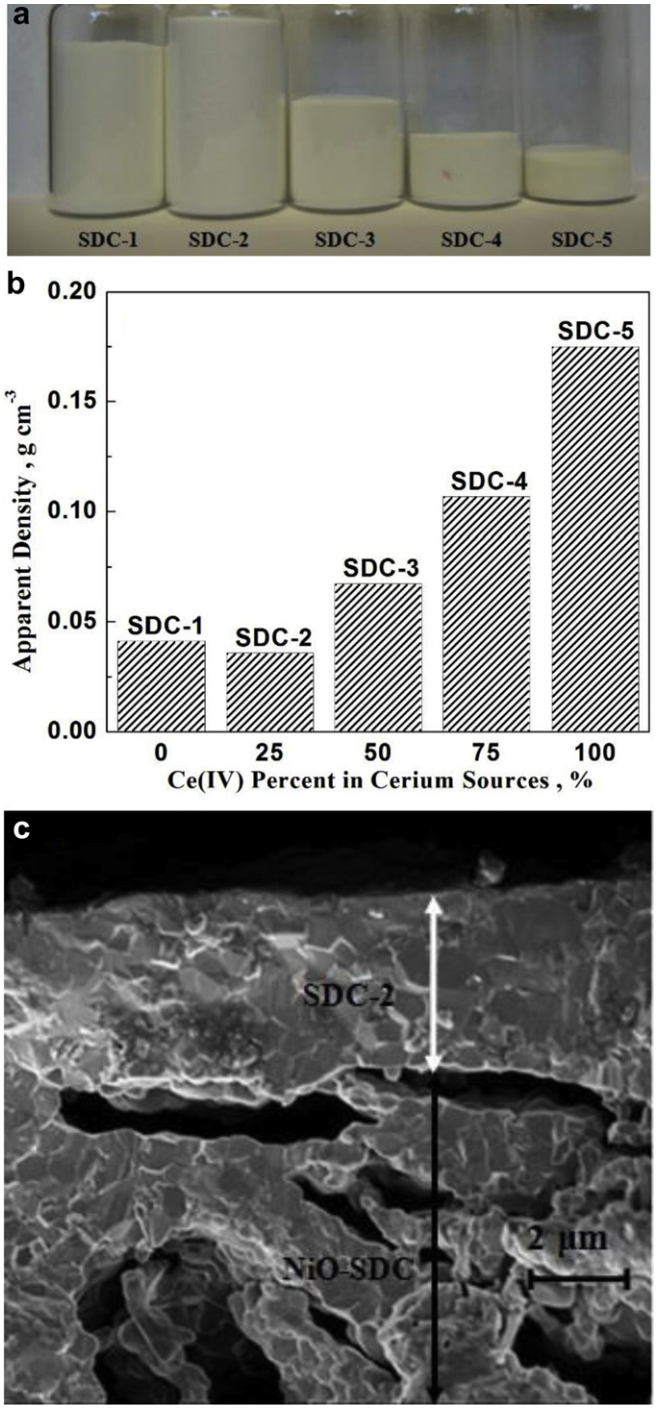

Fig. 3. (a) A visual comparison of the volumes of 1.00 g SDC powders derived from different cerium sources (all bottles are the same size), (b) the estimated apparent densities of different SDC powders, (c) SEM image of a cross-sectional view of a 4-μm-thick SDC-2 electrolyte membrane supported on a NiO–SDC substrate fabricated using a co-pressing and co-sintering process.

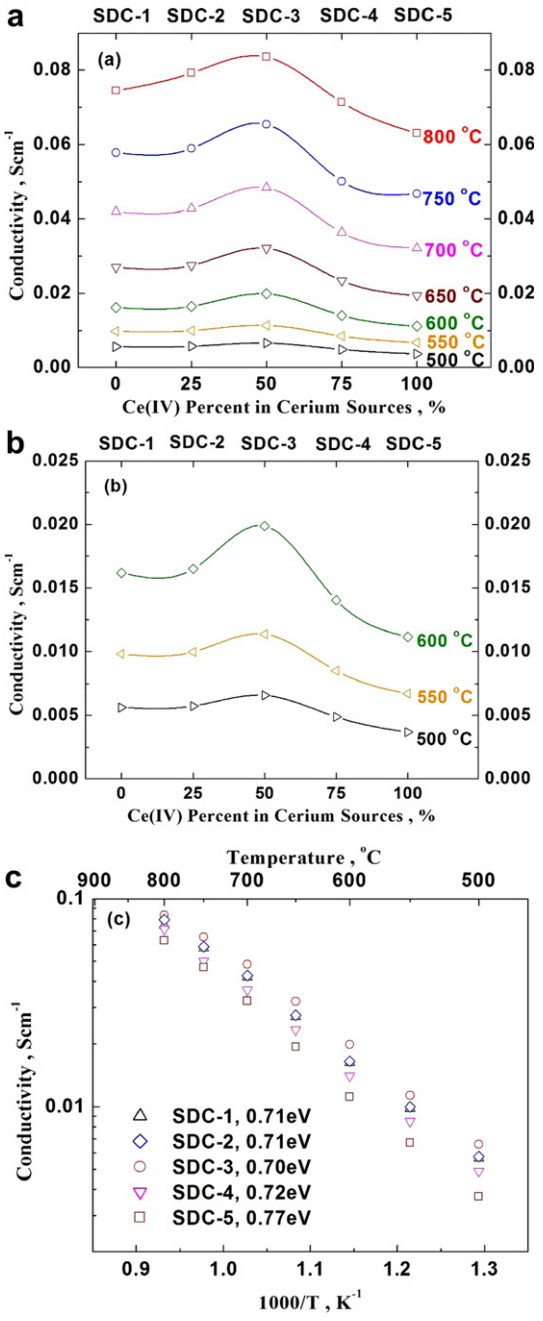

Fig. 4. Conductivity of SDC pellets sintered at 1400 °C for 5 h with different SDC powders: (a) conductivities versus cerium sources (500–800 °C), (b) conductivities versus cerium sources (500–600 °C) and (c) conductivities versus testing temperatures.

with increasing the content of $Ce(NO_3)_3$ used in the precursor mixtures.

As is well known, ionic conductivities of doped CeO_2 depend on the type and amount of dopants and the microstructure (e.g., density, grain boundary, grain size and shape as well as their distributions) of the electrolyte [30–38]. Since all samples in this study are SDC with the same composition and prepared using the same synthesis process (GNP), the microstructure must play an important role in ionic conduction. Fig. 5 shows some typical microstructures (SEM images) of the samples sintered at 1400 °C for 5 h. The SEM samples were prepared by grinding and polishing, followed by thermal etching (at 1000 °C for 2 h) to reveal the details of the microstructure. While all the samples are relatively dense, the average grain size and size distribution of the samples are influenced by the precursors used. Clearly, the samples with larger grain sizes exhibited higher conductivities (Fig. 4), indicating that the grain boundary resistance makes more contribution to the total resistances of the SDC samples of smaller grains. This is consistent with previous studies [9,32,39–41].

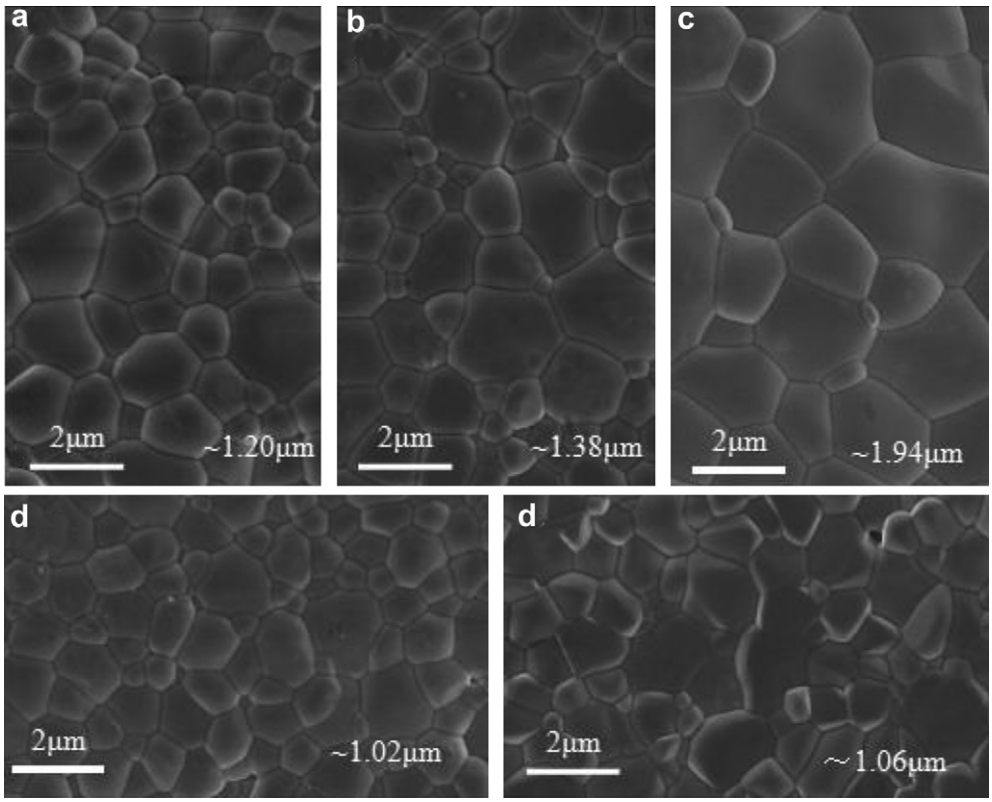

Fig. 5. Typical microstructures (SEM images) of the SDC samples sintered at 1400 °C for 5 h after grinding, polishing, and thermal etching (at 1000 °C for 2 h): (a) SDC-1, (b) SDC-2, (c) SDC-3, (d) SDC-4, and (e) SDC-5.

3.3. Application in single cells

To evaluate the electrochemical performance of these SDC powders as electrolyte in real SOFC systems, single cells were fabricated and characterized using Ni/SDC (65 wt%:35 wt%) anodes and SSC/SDC (70 wt%:30 wt%) cathodes. For brevity, the single cells prepared using different SDC powders (e.g., SDC-1, SDC-2, SDC-3, SDC-4 and SDC-5) as the electrolyte are referred as Cell-1, Cell-2, Cell-3, Cell-4, and Cell-5, respectively (Table 1). Shown in Fig. 6 are a cross-sectional and a surface view of the electrolyte membrane of Cell-3 co-fired at 1250 °C for 5 h. The electrolyte membrane appears to be dense, indicating that the synthesized powder is suitable for the fabrication of anode-supported cells using a co-pressing and co-firing process.

Fig. 7(a) presents some typical current–voltage curves of these cells operated at 600 °C with wet hydrogen (3% H_2O) as the fuel and ambient air as the oxidant. Each cell exhibited an open circuit voltage (OCV) of 0.895 ± 0.002 V, which is rather high for an SOFC based on SDC electrolyte at this temperature [26,42], suggesting that very dense electrolyte membranes were obtained. On the other hand, the peak power densities of Cell-1, Cell-2, Cell-3, Cell-4, and Cell-5 are 0.666, 0.694, 0.725, 0.639, and 0.607 W cm^{-2}, respectively. The trend in cell performance seems to be consistent with that of the conductivity of the SDC powders used as the electrolytes. To provide more detailed information, typical electrochemical impedance spectra of these cells were acquired under open circuit conditions with a two-electrode configuration, as shown in Fig. 7(b). The ohmic resistances of the cells can be obtained form the high frequency intercepts with the real axis in Fig. 7(b), and the total polarization resistances Rp were determined from the equation below [43]:

$$R_p = \frac{R_t - R_\Omega}{\frac{V_{oc}}{En}\left[1 - \frac{R_\Omega}{R_t}\left(1 - \frac{V_{oc}}{En}\right)\right]} \quad (7)$$

where *En* is the Nernst potential at 600 °C, V_{oc} is the OCV, R_Ω is the ohmic resistance, and R_t is the total resistance of the cell (determined from the low frequency intercept with the real axis in Fig. 7(b)). The calculated R_p and R_Ω for each cell are then plotted in Fig. 7(c). As is shown in the figure, the calculated R_p values of the cells are very similar, which are about 0.311 ± 0.003 Ω cm^2. On the other hand, significant differences in ohmic resistances were observed. For example, the ohmic resistance of Cell-3 was only 0.119 Ω cm^2, but it increased to 0.147 Ω cm^2 when SDC-5 powders were used as the electrolyte. Further, considering the fact that the OCVs of all test cells are similar, the differences among the cell performance must be attributed to the variation in ionic conductivities of the electrolytes, which can also be seen from the difference in the slopes of the *V–I* curves shown in Fig. 7(a).

Since Cell-3 displayed the best performance among all cells tested, the performance of this cell was further tested at different temperatures, as shown in Fig. 8. The OCV decreased from 0.934 to 0.855 V as the operation temperature was raised from 550 to 650 °C, demonstrating peak power densities of 0.461, 0.725, and 0.996 W cm^{-2} at 550, 600, and 650 °C, respectively (Fig. 8(a)). The electrochemical impedance spectra of the cell measured at different temperatures are shown in Fig. 8(b).

3.4. Discussion

As reported in the literature, the glycine/nitrate ratio and calcination temperature have significant effects on the properties of SDC powders derived from a GNP [12,14,24,25]. In this study, it is demonstrated that cerium source is another important factor that critically impact the properties of SDC powders. It appears that $Ce(NO_3)_3$ is a better cerium source than $Ce(NH_4)_2(NO_3)_6$ in the GNP, producing SDC-1 powders with lower apparent density, higher ionic conductivity, and lower activation energy for electrical

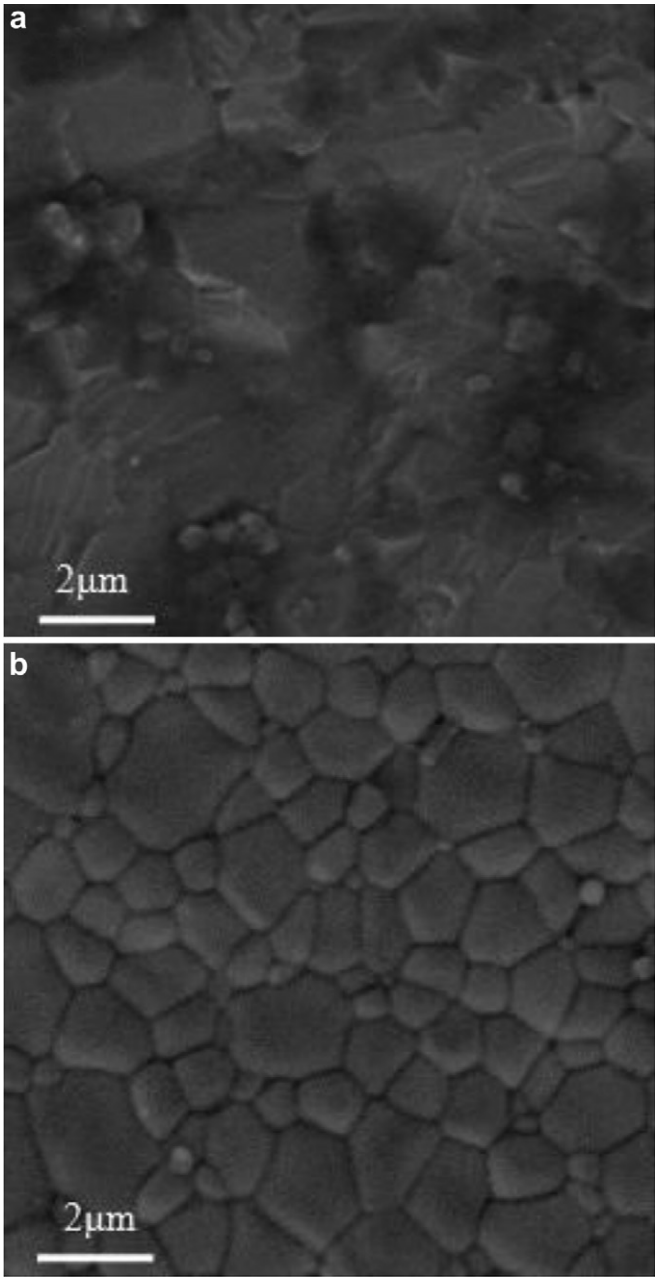

Fig. 6. (a) A cross-sectional and (b) a surface view of the electrolyte membrane of Cell-3 co-fired at 1250 °C for 5 h.

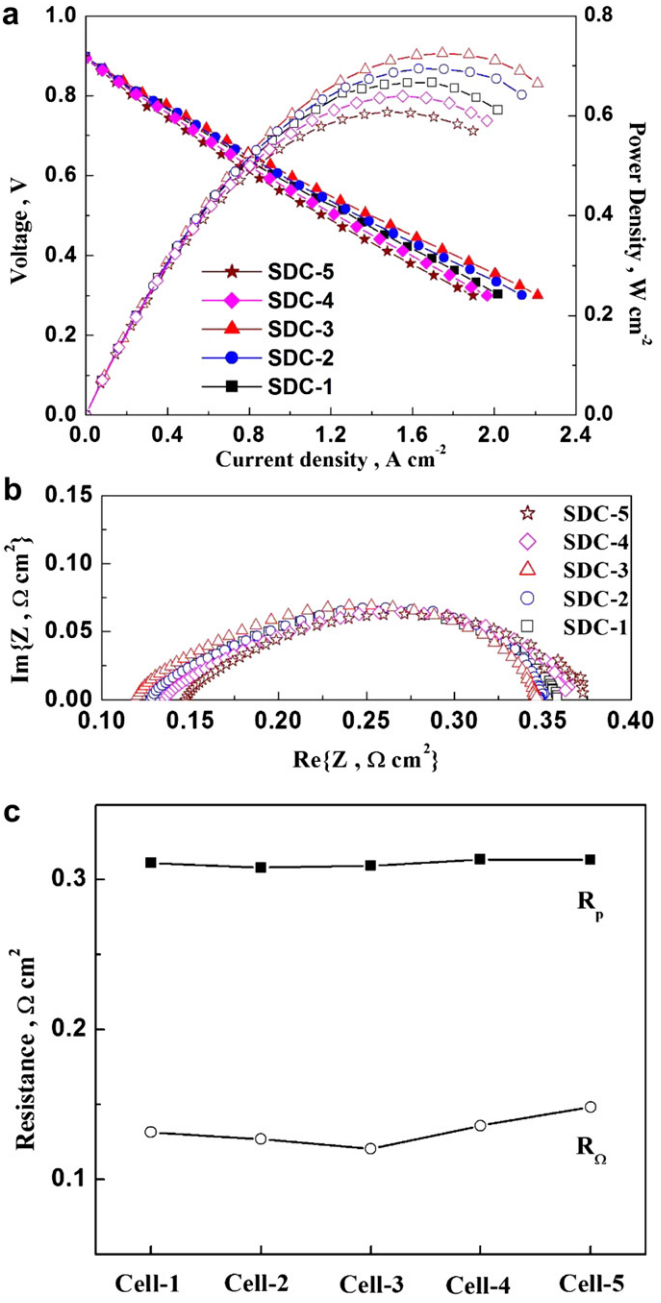

Fig. 7. (a) Dependence of cell voltage and power density on current density, (b) impedance spectra measured under open circuit conditions, (c) R_Ω and calculated R_p, for different cells tested at 600 °C, when humidified H_2 (3% H_2O) and ambient air are used as the fuel and the oxidant, respectively.

conduction. Consequently, single cell with SDC-1 as the electrolyte showed higher performance than that with SDC-5 under the same operating conditions (when the same anode and cathode materials were applied using identical fabrication processes).

On the other hand, although $Ce(NH_4)_2(NO_3)_6$ seems to be a less favorable choice as the single cerium source for GNP synthesis of SDC powders, the combination of $Ce(NH_4)_2(NO_3)_6$ and $Ce(NO_3)_3$ as mixed starting materials produced higher quality SDC powders. For example, SDC-2 powders synthesized with 25 mol% $Ce(NH_4)_2(NO_3)_6$ + 75 mol% $Ce(NO_3)_3$ as the cerium source exhibited even lower apparent density and higher ionic conductivities than the SDC-1 powders derived from single $Ce(NO_3)_3$. In particular, when 50 mol% $Ce(NH_4)_2(NO_3)_6$ + 50 mol% $Ce(NO_3)_3$ were used as the starting materials, the synthesized SDC-3 powders showed the highest ionic conductivities, the lowest activation energy for electrical conduction, and the highest potential for fabrication of thin-film membrane based high-performance cells [12,17,29,37,44–46].

When anode-supported single cells were fabricated using a co-pressing and co-sintering process, the electrolyte membranes prepared with SDC-1 and SDC-2 powders had very high relative densities, attributed primarily to the relatively low apparent densities of the SDC powders used. For the cells fabricated from other SDC powders, Cell-3, Cell-4, and Cell-5, the electrolyte membranes are sufficiently dense to obtain OCVs as high as those of Cell-1 and Cell-2, but some voids are observable on the cross-

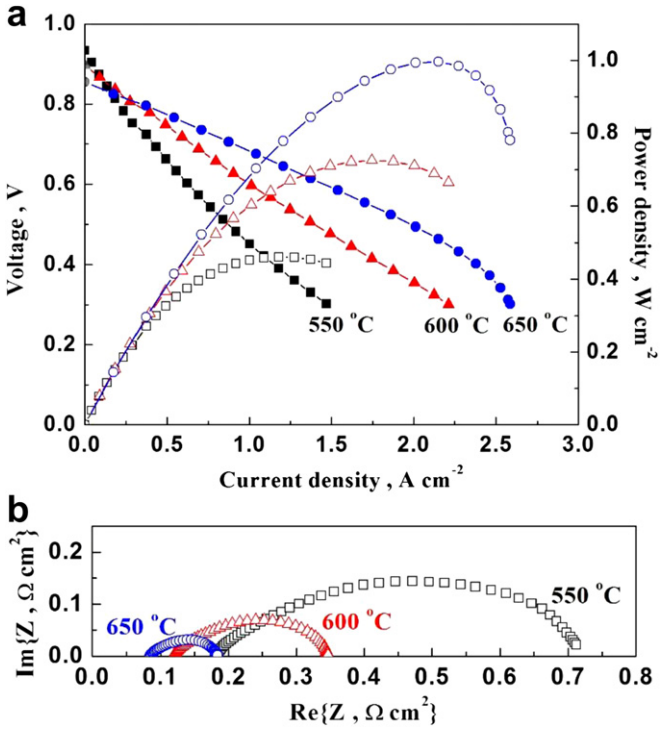

Fig. 8. (a) Dependence of cell voltage and power density on current density and (b) impedance spectra measured under open circuit conditions, for Cell-3 tested at 550, 600 and 650 °C, when humidified H_2 (3% H_2O) and ambient air are used as the fuel and the oxidant, respectively.

sectional views. Since the same processes were used to fabricate the electrodes for all test cells, the differences in cell performance are attributed mainly to the resistances of the electrolyte membranes. It is noted that the electrolyte thicknesses of the cells are also very close to each other (22.5 ± 0.5 μm), as the same amount of SDC powders (by weight) were used for each electrolyte. Thus, the differences in cell performance are most likely originated from the difference in the effective ionic conductivities of the SDC membranes derived from different cerium sources.

In particular, the electrolyte membranes derived from the SDC-3 powders showed the highest conductivities and the corresponding cells demonstrated a peak power density of 0.725 W cm^{-2} at 600 °C, representing the best performance for SDC based SOFCs fabricated by co-pressing and co-firing without any electrode optimizations. Also, compared with Cell-5, the performance enhancement of Cell-3 is about 19.4%, a significant effect only by optimization of electrolyte powder synthesis. On the other hand, the SDC-2 powders are most favorable for fabrication of thin-film SDC-layers due to its lowest apparent density. The ultra-thin layers may play very important roles in bi-layer electrolytes and buffer layers fabrications.

4. Conclusion

In summary, proper combination of $Ce(NO_3)_3$ and $Ce(NH_4)_2(NO_3)_6$ as mixed cerium source is shown to be more effective in achieving SDC powders with low apparent density for easy fabrication of thin-film electrolyte membrane with very high sintered density and excellent ionic conductivity. In particular, when 50 mol% $Ce(NO_3)_3$ + 50 mol% $Ce(NH_4)_2(NO_3)_6$ are used as the starting material, SDC powders derived from the GNP can be readily densified to achieve high ionic conductivities, thus being the most conducive electrolyte for IT-SOFCs. On the other hand, SDC powders derived from a mixture consisting of 75 mol% $Ce(NO_3)_3$ and 25 mol% $Ce(NH_4)_2(NO_3)_6$ exhibit the lowest apparent density and also reasonably high ionic conductivities, thus being very promising for fabrication of thin-film electrolyte membranes.

Acknowledgment

This material is based upon work supported as part of the Heterogeneous Functional Materials (HetroFoaM) Center, an Energy Frontier Research Center funded by the U.S. Department of Energy, Office of Science, Office of Basic Energy Sciences under Award Number DE-SC0001061. Zhangbo Liu thanks the fellowship support by the China Scholarship Council.

References

[1] B.C.H. Steele, A. Heinzel, Nature 414 (6861) (2001) 345–352.
[2] Z.L. Zhan, S.A. Barnett, Science (2005) 844–847.
[3] Y.H. Huang, et al., Science (2006) 254–257.
[4] L. Yang, et al., Science (2009) 126–129.
[5] Z. Cheng, et al., Energy & Environmental Science 4 (11) (2011) 4380–4409.
[6] M. Liu, et al., Materials Today 14 (11) (2011) 534–546.
[7] M. Liu, et al., Nano Energy 1 (3) (2012) 448–455.
[8] M. Mogensen, N.M. Sammes, G.A. Tompsett, Solid State Ionics 129 (1–4) (2000) 63–94.
[9] B. Steele, Solid State Ionics 129 (1–4) (2000) 95–110.
[10] C. Xia, M. Liu, Journal of the American Ceramic Society 84 (8) (2001) 1903–1905.
[11] C. Xia, M. Liu, Solid State Ionics 144 (3–4) (2001) 249–255.
[12] R. Peng, et al., Materials Letters 56 (6) (2002) 1043–1047.
[13] C. Xia, M. Liu, Solid State Ionics 152–153 (2002) 423–430.
[14] T. Mokkelbost, et al., Chemistry of Materials 16 (25) (2004) 5489–5494.
[15] K. Singh, S. Acharya, S. Bhoga, Ionics 12 (4) (2006) 295–301.
[16] S.B. Bošković, et al., Ceramics International 34 (8) (2008) 2001–2006.
[17] R. Tian, et al., Solid State Ionics 192 (1) (2011) 580–583.
[18] L.A. Chick, et al., Materials Letters 10 (1–2) (1990) 6–12.
[19] Z.L. Wang, X. Feng, The Journal of Physical Chemistry B 107 (49) (2003) 13563–13566.
[20] C.-C. Hwang, et al., Materials Science and Engineering: B 132 (3) (2006) 229–238.
[21] P. Singh, M.S. Hegde, Journal of Solid State Chemistry 181 (12) (2008) 3248–3256.
[22] Q. Yuan, et al., Journal of Colloid and Interface Science 335 (2) (2009) 151–167.
[23] R.I. Walton, Progress in Crystal Growth and Characterization of Materials 57 (4) (2011) 93–108.
[24] T. Pine, et al., Journal of the American Ceramic Society 90 (12) (2007) 3735–3740.
[25] R.D. Purohit, et al., Materials Research Bulletin 36 (15) (2001) 2711–2721.
[26] Z. Liu, et al., Journal of Power Sources 196 (20) (2011) 8561–8567.
[27] C. Xia, et al., Solid State Ionics 149 (1–2) (2002) 11–19.
[28] L.A. Chick, et al., Material Research Society Symposium Proceedings (1991) 159–164.
[29] Q. Liu, et al., The Journal of Physical Chemistry C 113 (39) (2009) 17262–17267.
[30] H. Yahiro, et al., Journal of Applied Electrochemistry 18 (4) (1988) 527–531.
[31] H. Inaba, H. Tagawa, Solid State Ionics 83 (1–2) (1996) 1–16.
[32] V.V. Kharton, et al., Journal of Materials Science 36 (5) (2001) 1105–1117.
[33] T. Mori, et al., Solid State Ionics 175 (1–4) (2004) 641–649.
[34] T. Mori, et al., Journal of the American Ceramic Society 88 (7) (2005) 1981–1984.
[35] F. Ye, et al., Journal of Applied Physics 101 (11) (2007) 113528–113535.
[36] D. Ding, et al., Solid State Ionics 179 (21–26) (2008) 896–899.
[37] D. Ding, et al., Electrochimica Acta 55 (15) (2010) 4529–4535.
[38] S.A. Acharya, Journal of Power Sources 198 (0) (2012) 105–111.
[39] X. Guo, J. Maier, Journal of Electrochemical Society (2001) E121–E126.
[40] X. Guo, R. Waser, Progress in Materials Science 51 (2) (2006) 151–210.
[41] T.S. Zhang, et al., Solid State Ionics 177 (13–14) (2006) 1227–1235.
[42] X. Zhang, et al., Journal of Power Sources 160 (2) (2006) 1211–1216.
[43] M. Liu, H. Hu, Journal of the Electrochemical Society (1996) L109–L112.
[44] M. Chen, et al., Ceramics International 35 (4) (2009) 1335–1343.
[45] S.L. Reis, E.C.C. Souza, E.N.S. Muccillo, Solid State Ionics 192 (1) (2011) 172–175.
[46] R. Sanghavi, et al., Solid State Ionics 204–205 (2011) 13–19.